Liver-specific paraoxonase-1 alleviates regulatory T cell-driven immunosuppression via metabolic reprogramming in hepatocellular carcinoma

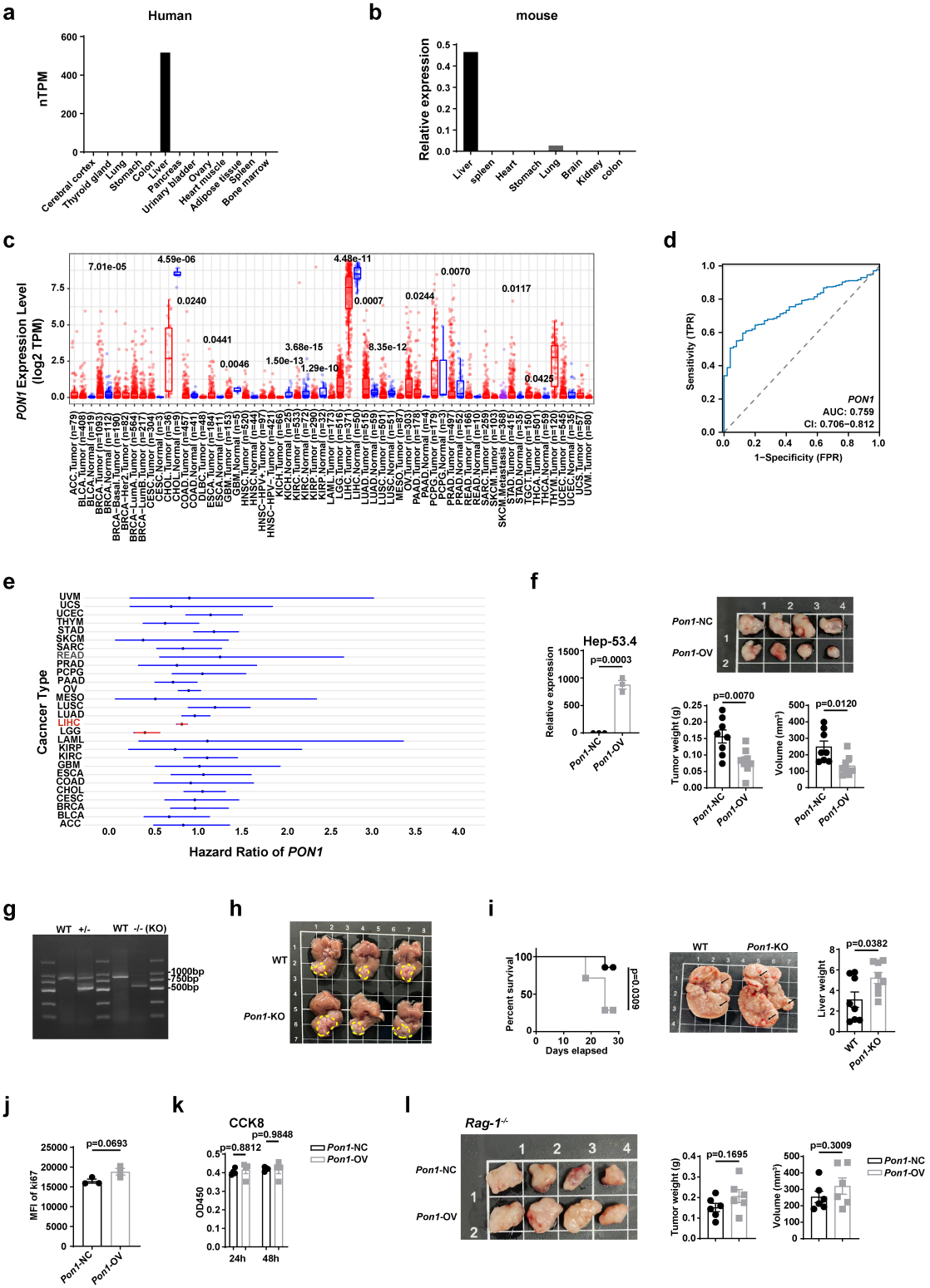
Zhou Lu, Huanchen Shi, Rongshan Gao, Chengjie zhong, Wei Zhang, Jian Zhu, Jianhang Huang, Ronghua Liu, Yun Xing, Yiwei Chu, Haixiang Sun, Guoming Shi, Aiwu Ke, Jian Zhou, Jiabin Cai, Jia Fan, Pingting Gao, Cheng Huang

Supplementary Figures and legends

Supplementary Tables

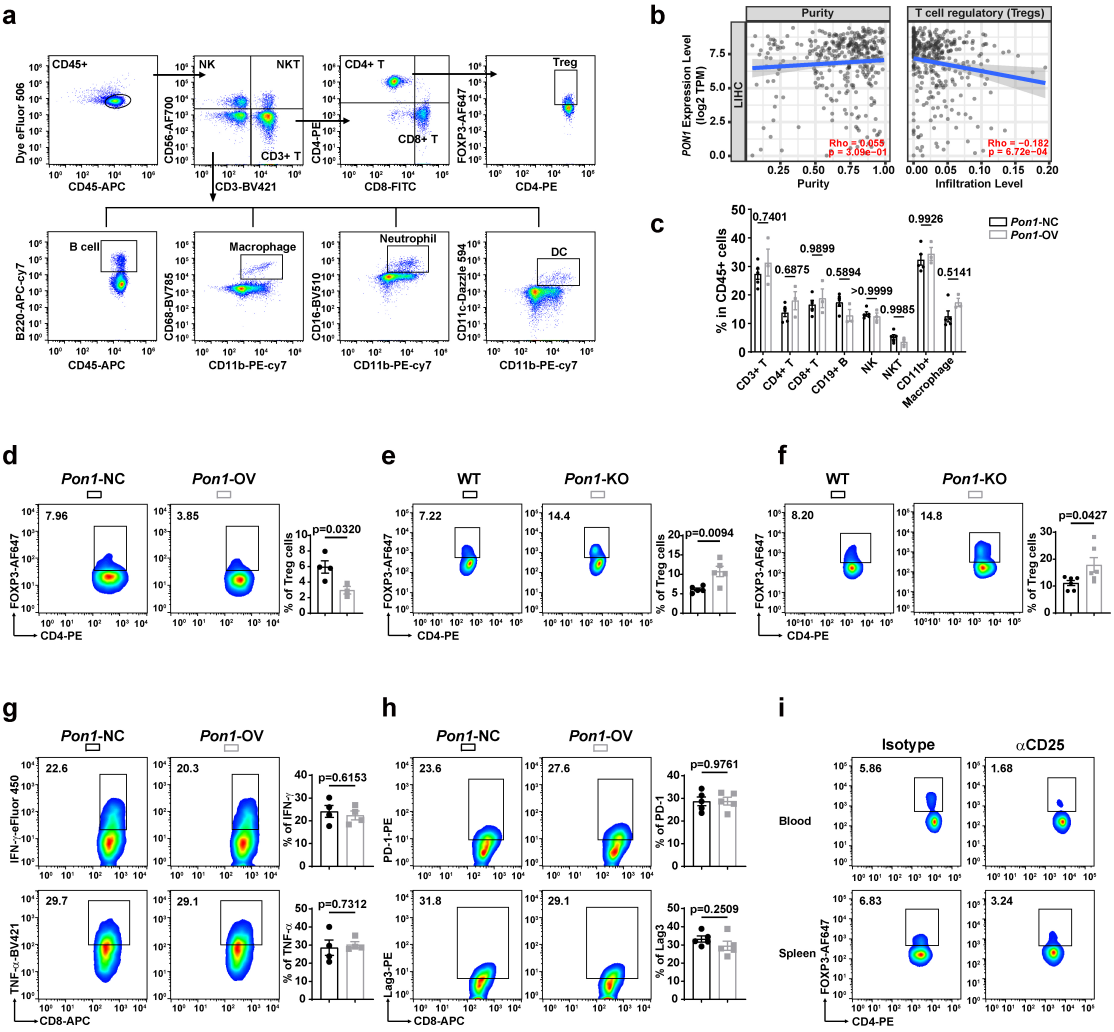
Supplementary Figures and legends

Supplementary Fig. 1



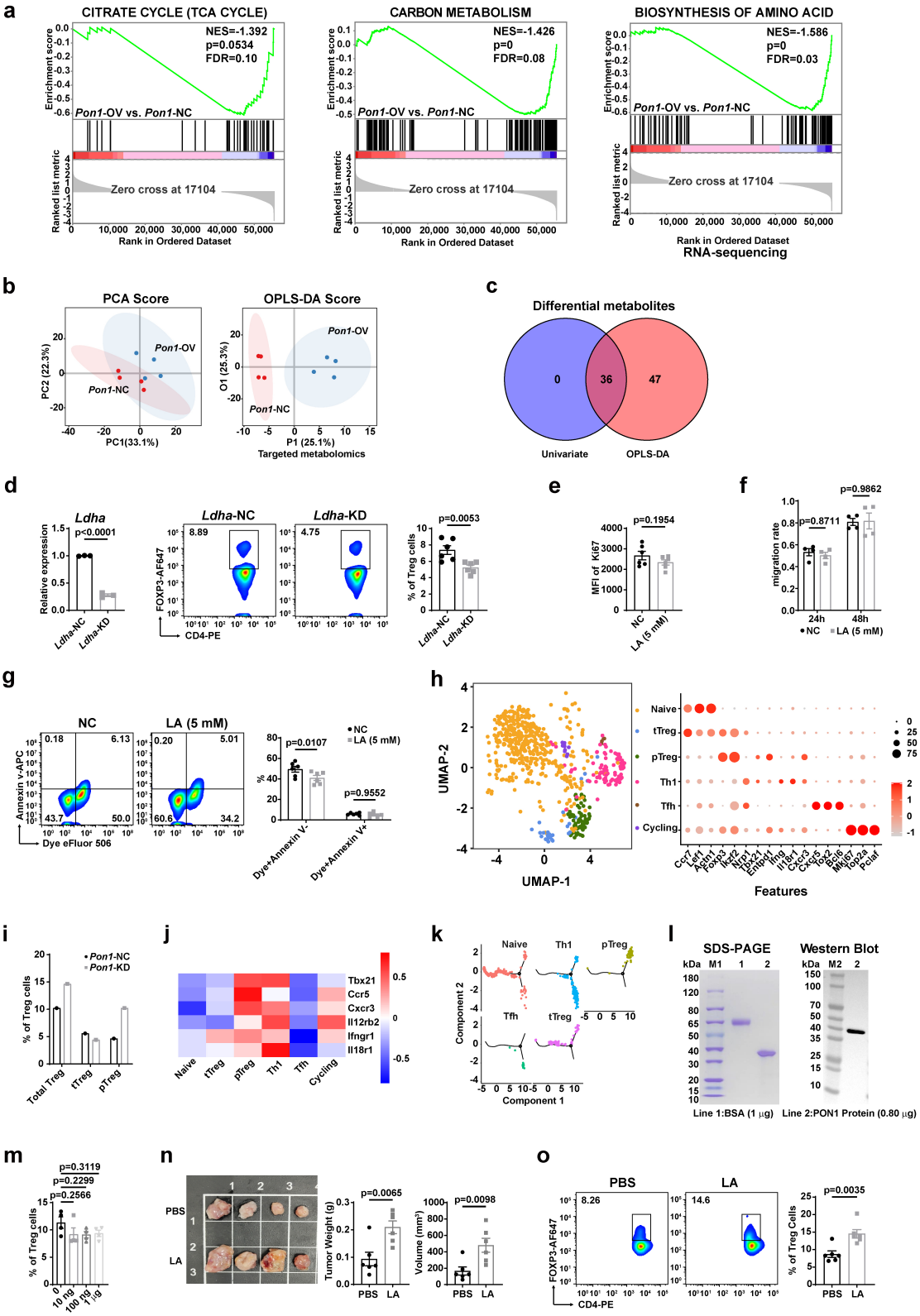
Supplementary Fig. 1 Liver-specific PON1 expression shows no significant effect on cell proliferation. (**a**) Analysis of *PON1* expression in multiple human tissues using The Human Protein Atlas database. (**b**) *Pon1* expression was analyzed in various tissues of mice. (**c**) *PON1* expression was analyzed in pan-cancer datasets from TCGA. (**d**) ROC curve analysis of *PON1* for diagnosing HCC. (**e**) Correlations between *PON1* and overall survival in pan-cancer analysis. (**f**) *Pon1* expression in Hep-53.4 cells (n = 3 independent experiments, left). Representative images, tumor weights, and volumes of subcutaneous tumors in the *Pon1*-OV and *Pon1*-NC groups (n = 8 mice per group, right). (**g**) Genotype verification of *Pon1*-KO mice. (**h**) Tumor growth in livers of WT and *Pon1*-KO mice after orthotopic inoculation with Hepa1-6 cells (n = 3 mice per group). (**i**) Survival curves of WT and *Pon1*-KO mice (n = 7 mice per group) with spontaneous HCC (left). Representative liver tumor images and liver weights measured at the experimental endpoint (n = 8 mice per group, right). (**j**) Ki67 expression in *Pon1*-NC and *Pon1*-OV Hepa1-6 cells (n = 3 independent experiments). (**k**) Cell viability of *Pon1*-NC and *Pon1*-OV Hepa1-6 cells was determined via CCK-8 assay (n = 4 independent experiments). (**l**) Representative images, weights, and volumes of subcutaneous tumors in *Rag-1*$^{-/-}$ mice implanted with *Pon1*-NC and *Pon1*-OV Hepa1-6 cells (n = 6 mice per group). In the box plots, the center line represents the median, the box boundaries indicate the IQR, and the whiskers extend to 1.5 × IQR. Data are presented as median with IQR (**c**) and as mean ± SEM (**f**, **i**–**l**). Statistical significance was determined by Wilcoxon rank-sum test (**c**), two-tailed unpaired Student's t-test (**f**, **j**, **l**), or two-way ANOVA with Sidak's multiple comparisons test (**k**). Survival curves (panel **i**) were compared using the log-rank test and liver weights using a two-tailed unpaired t-test. TPM transcripts per million, CI confidence interval, AUC area under the curve, FPR false positive rate, TPR true positive rate, NC negative control, OV overexpression, WT wide type, KO knockout, MFI mean fluorescence intensity, CCK8 cell counting kit-8, ns not significant. Source data are provided as a Source Data file.

Supplementary Fig. 2



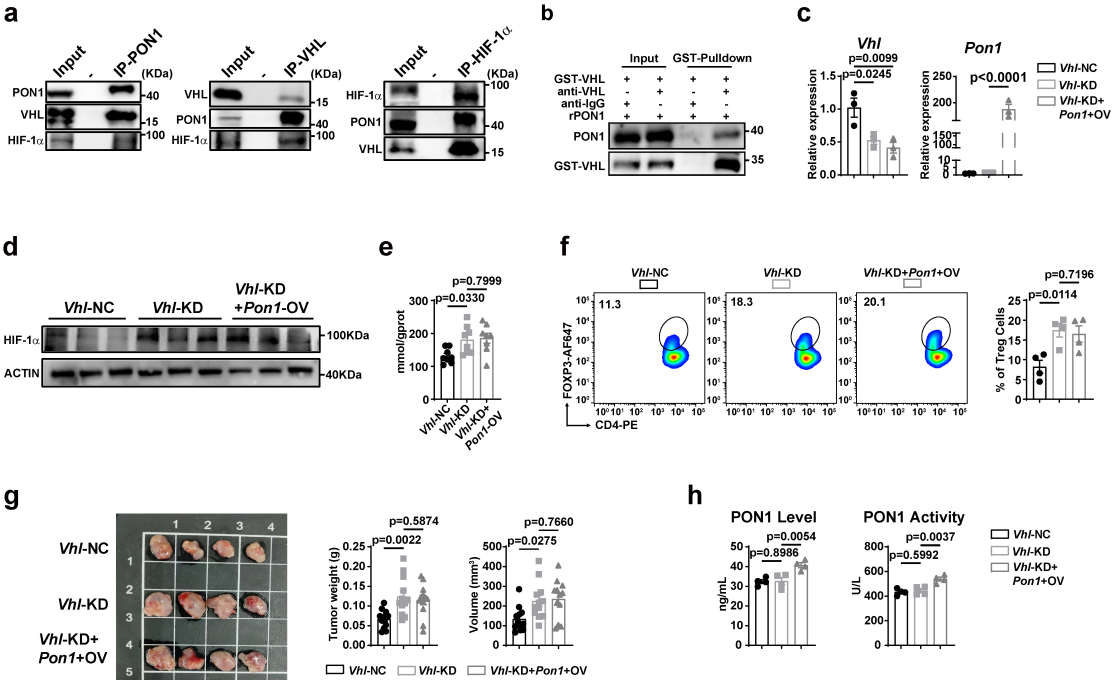
Supplementary Fig. 2 *PON1* expression in HCC cells is negatively related to Treg cell infiltration. (**a**) Gating strategy for tumor-infiltrating immune cells in Fig. 2b. (**b**) Correlation analysis between *PON1* expression and Treg cell infiltration level using the Tumor Immune Estimation Resource (TIMER) database. (**c**) The proportion of tumor-infiltrating immune cells in *Pon1*-NC tumors (n = 5 mice) and *Pon1*-OV subcutaneous tumors (n = 3 mice). (**d**) Treg cell percentages in orthotopic tumors from *Pon1*-NC (n = 4 mice) and *Pon1*-OV (n = 3 mice) Hepa1-6 cells. (**e**) Treg cell percentages in orthotopic Hepa1-6 tumors implanted in WT and *Pon1*-KO mice (n = 5 mice per group). (**f**) Treg cell percentages in WT and *Pon1*-KO mice with orthotopic HCC induced by hydrodynamic tail-vein injection (n = 6 mice per group). (**g**) $CD8^+$ T cells isolated from spleens by magnetic-activated cell sorting were co-cultured with either *Pon1*-NC or *Pon1*-OV Hepa1-6 cells in 48-well plates, supplemented with anti-CD3 (2 μg/mL) and anti-CD28 (2 μg/mL). IFN-γ and TNF-α expression in $CD8^+$ T cells was measured 48 h later (n = 4 independent experiments). (**h**) PD-1 and Lag3 expression on $CD8^+$ T cells after 48 h of co-culture (n = 5 independent experiments). (**i**) Analysis of the efficiency of Treg deletion in the blood and spleen by αCD25. Data are presented as mean ± SEM (**c**–**h**). Statistical significance was determined by two-way ANOVA with Sidak's multiple comparisons test (**c**) or two-tailed unpaired Student's t-test (**d**–**h**). NK natural killer cell, NKT natural killer T cell, DC dendritic cell, Treg regulatory T cell, NC negative control, OV overexpression, WT wide type, KO knockout, ns not significant. Source data are provided as a Source Data file.

Supplementary Fig. 3



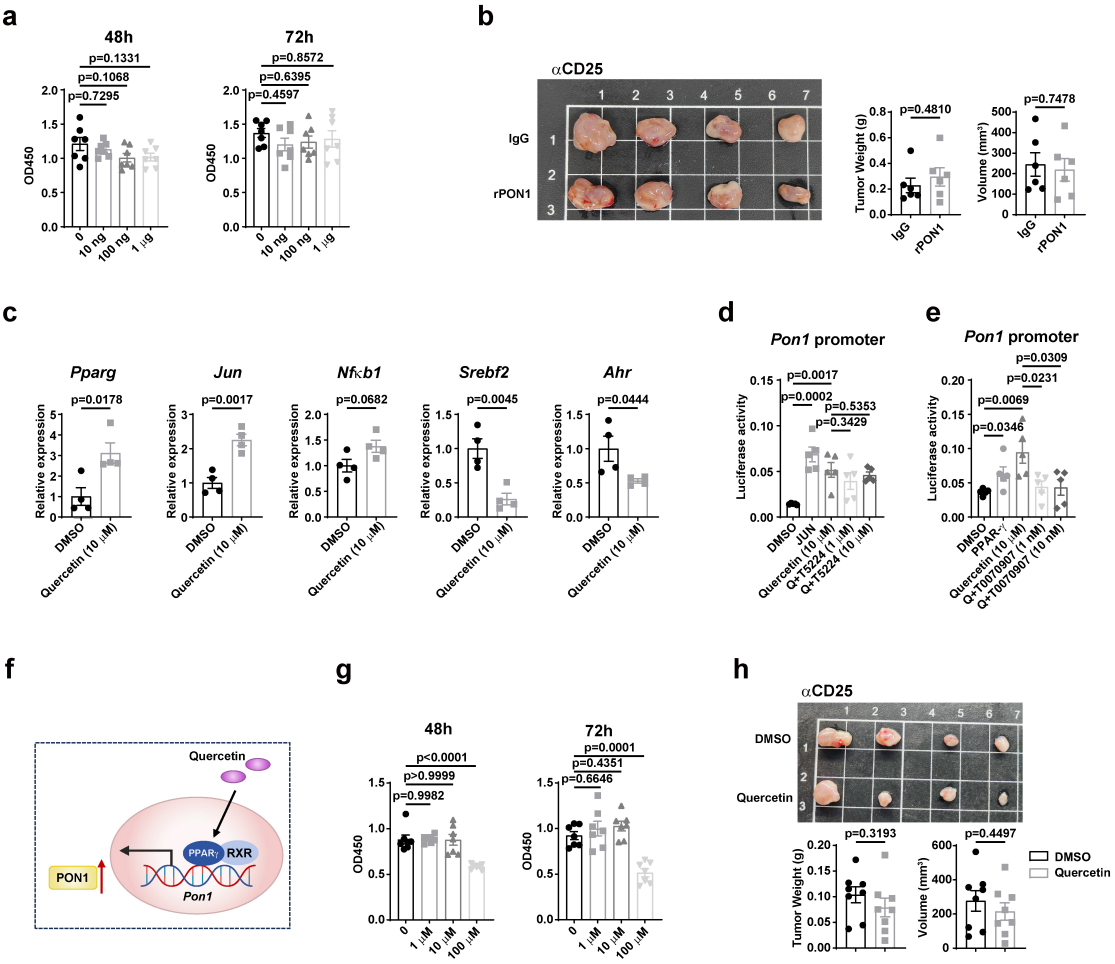
Supplementary Fig. 3 Regulation of Treg cell fate by lactic acid. (**a**) Enriched metabolic pathways identified via GSEA using DEGs in *Pon1*-NC and *Pon1*-OV subcutaneous tumors. (**b**) Metabolomic analysis of *Pon1*-NC and *Pon1*-OV subcutaneous tumors using principal component analysis (PCA) and orthogonal partial least squares-discriminant analysis (OPLS-DA). (**c**) Venn diagram of differential metabolites screened by multivariate versus univariate analyses. (**d**) The expression of *Ldha* in Hepa1-6 cells (n = 3 independent experiments), and its effect on Treg cell differentiation (n = 6 independent experiments). (**e**–**g**) Effects of lactic acid treatment on Treg cell proliferation (n = 6 independent experiments), migration (n = 4 independent experiments), and apoptosis (n = 6 independent experiments). (**h**) Clustering and marker genes of $CD4^+$ T cells in single cell sequencing data from Hepa1-6-derived tumors. (**i**) Proportions of Treg cell subtypes in *Pon1*-NC and *Pon1*-KD subcutaneous tumors. (**j**) Expression of Th1 signature genes across $CD4^+$ T Cell subsets. (**k**) Pseudotemporal analysis of $CD4^+$ T Cell subsets. (**l**) Purification and characterization of rPON1. (**m**) Treg cell percentages in groups treated with different rPON1 concentrations (n = 4 independent experiments). (**n**) Representative images, weight, and volume of subcutaneous tumors from mice treated with or without lactic acid (n = 6 mice per group). (**o**) Treg cell percentages in subcutaneous tumors treated with or without lactic acid (n = 6 mice per group). Data are presented as mean ± SEM (**d**–**g**, **m**–**o**). Statistical significance was determined by permutation test (**a**), two-tailed unpaired Student's t-test (**d**, **e**, **n**, **o**), two-way ANOVA with Sidak's multiple comparisons test (**f**–**g**), or one-way ANOVA with Dunnett's test (**m**). NES normalized enrichment score, FDR false discovery rate, PCA principal component analysis, OPLS-DA orthogonal projections to latent structures-discriminant analysis, vs. versus, NC negative control, KD knockdown, LA lactic acid, MFI mean fluorescence intensity, ns not significant, Th1 T helper 1 cell, Tfh T follicular helper cell, Treg regulatory T cell, tTreg thymus-derived Treg, pTreg peripherally induced Treg, BSA bovine serum albumin, PBS phosphate-buffered saline. Source data are provided as a Source Data file.

Supplementary Fig. 4



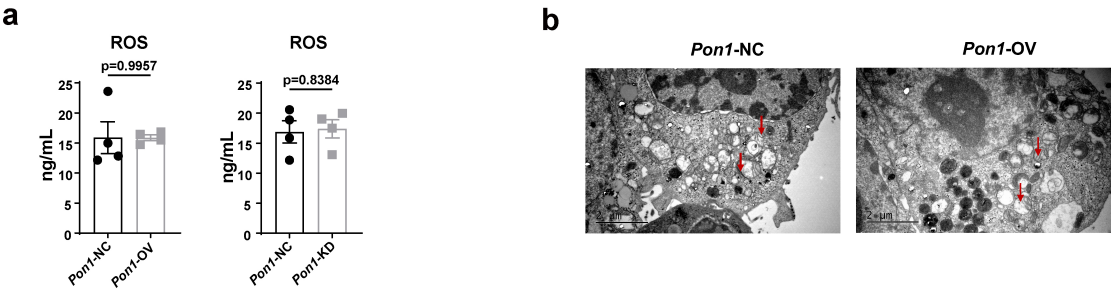
Supplementary Fig. 4 VHL biding is essential for the anti-tumor effects of PON1. (**a**) Co-IP of exogenously expressed PON1, VHL, and HIF-1α in Hepa1-6 cells exposed to hypoxia. The samples derive from the same experiment but different gels for PON1, another for VHL, and another for HIF-1α were processed in parallel. (**b**) GST pull-down results of the interaction between PON1 and VHL. The samples derive from the same experiment but different gels for PON1 and another for GST-VHL were processed in parallel. (**c**) *Vhl* and *Pon1* expression in Hepa1-6 cells with different treatments (n = 3 independent experiments). Subcutaneous tumors established using Hepa1-6 cells with *Vhl* knockdown, with or without *Pon1* overexpression. (**d**–**f**) HIF-1α protein levels (n = 3 mice per group), lactic acid concentrations (n = 8 mice per group), and Treg cell proportions (n = 4 mice per group) in subcutaneous tumors from the different groups. (**g**) Representative images, weights, and volumes of subcutaneous tumors from the different groups (n = 12 mice per group). (**h**) Serum PON1 levels and activity in tumor-bearing mice from the different groups (n = 4 mice per group). Data (**c**, **e**–**h**) are presented as mean ± SEM. Statistical significance was determined by one-way ANOVA with Dunnett's test (**c**) or one-way ANOVA with Holm-Sidak's multiple comparisons test (**e**–**h**). Data in panels **a** and **b** are representative of two independent experiments. IP immunoprecipitation, GST Glutathione S-transferases, rPON1 recombinant PON1 protein, NC negative control, KD knockdown, OV overexpression, ns not significant, Treg regulatory T cell. Source data are provided as a Source Data file.

Supplementary Fig. 5



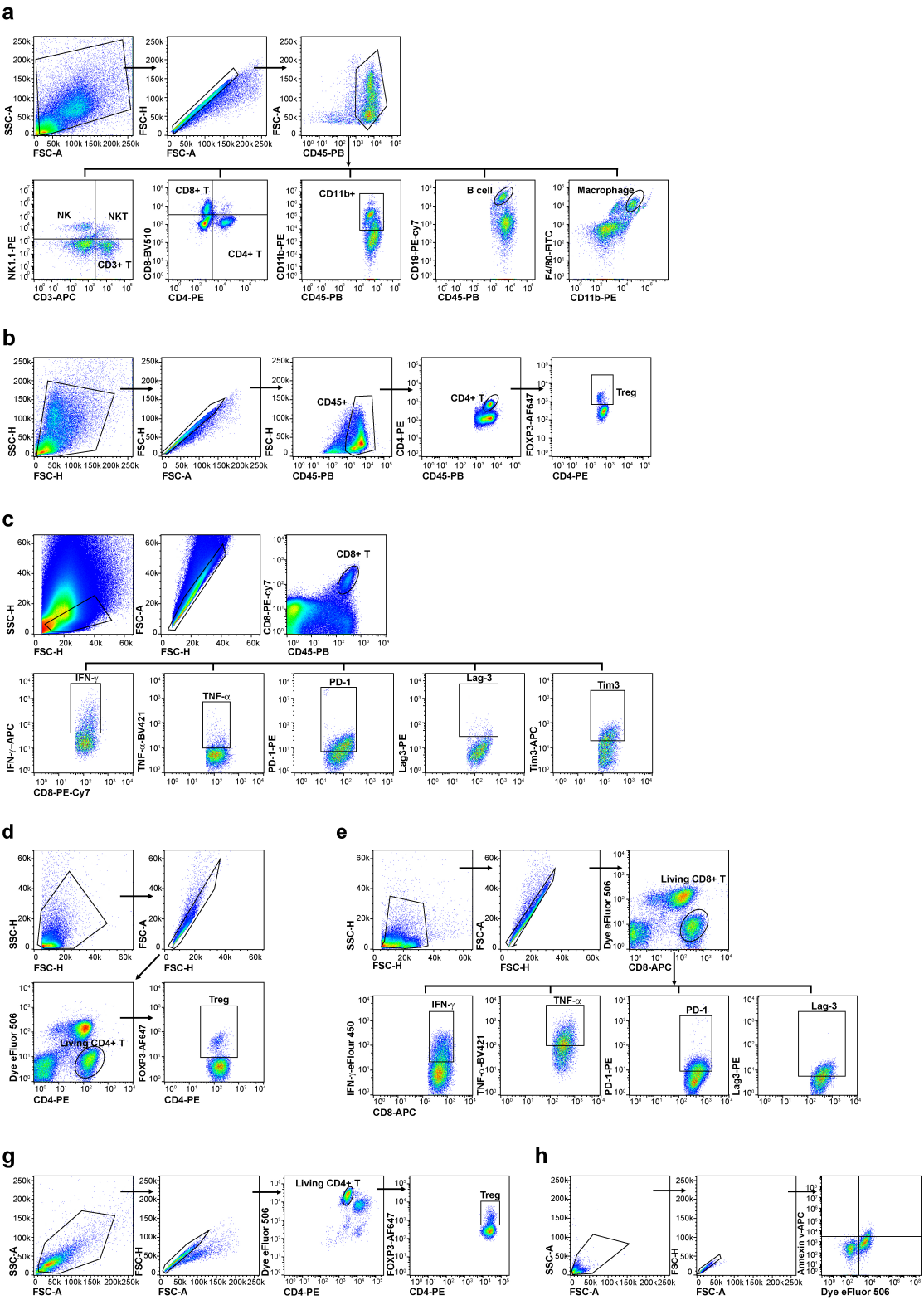
Supplementary Fig. 5 PPARγ-mediated upregulation of *Pon1* expression by quercetin. (**a**) Cell viability of Hepa1-6 cells treated with different rPON1 concentrations (n = 7 independent experiments). (**b**) Representative images, weights, and volumes of subcutaneous tumors from Treg-depleted mice treated with or without rPON1 (n = 6 mice per group). (**c**) Expression of *Pparg*, *Jun*, *Nfκb1*, *Srebf2*, *Ahr* and *Sp1* in Hepa1-6 cells treated with quercetin (10 μM, n = 4 independent experiments). *Sp1* was undetectable in our assays and excluded from data reporting. (**d**) Luciferase activity of the *Pon1* promoter in Hepa1-6 cells treated with *Jun* plasmid, quercetin, or quercetin combined with the JUN antagonist (T5224, n = 5 independent experiments). (**e**) Luciferase activity of the *Pon1* promoter in Hepa1-6 cells treated with *Pparg* plasmid, quercetin, or quercetin combined with the PPARγ antagonist (T0070907, n = 5 independent experiments). (**f**) Schematic diagram of quercetin regulating *Pon1* Expression. (**g**) Cell viability of Hepa1-6 cells treated with different quercetin concentrations (n = 7 independent experiments). (**h**) Representative images, weights, and volumes of subcutaneous tumors from Treg-depleted mice treated with or without quercetin (n = 8 mice per group). Data are presented as mean ± SEM (**a**–**e**, **g**–**h**). Statistical significance was determined by one-way ANOVA with Dunnett's test (**a**, **g**) and two-tailed unpaired Student's t-test (**b**–**e**, **h**). rPON1 recombinant PON1 protein, ns not significant. Source data are provided as a Source Data file.

Supplementary Fig. 6



Supplementary Fig. 6 PON1 has no effects on reactive oxygen species production in Hepa1-6 cells. (**a**) ROS levels in control, *Pon1*-OV, and *Pon1*-KD Hepa1-6 cells (n = 4 independent experiments). (**b**) Mitochondrial structures of *Pon1*-NC and *Pon1*-OV Hepa1-6 cells. Scale bar: 2 μm. Data are presented as mean ± SEM (**a**). Statistical significance was determined by two-tailed unpaired Student's t-test (**a**). Data in panel **b** are representative of two independent experiments. NC negative control, KD knockdown, OV overexpression, ROS reactive oxygen species, ns not significant. Source data are provided as a Source Data file.

Supplementary Fig. 7



Supplementary Fig. 7 Gating Strategy for flow cytometry. (**a**) Gating strategy for tumor-infiltrating immune cells in Supplementary Fig. 2c. (**b**) Gating strategy for Treg cells in the tumor in Figs. 2d, 2f, 3n, 5f, 6c, 6g and supplementary Figs. 2d–f, 2i, 3o and 4f. (**c**) Gating strategy for expression of IFN-γ, TNF-α, PD-1, Lag3, Tim3 in in tumor-infiltrating $CD8^+$ T cells, related to Figs. 2e and 2g. (**d**) Gating strategy for Treg cells in the co-culture experiment of Fig. 2i and Supplementary Fig. 3d. (**e**) Gating strategy for expression of IFN-γ, TNF-α, PD-1, Lag3, Tim3 in $CD8^+$ T cells from the co-culture experiment in Supplementary Figs. 2g–h. (**f**) Gating strategy for Treg cells from *in vitro* culture, related to Fig. 3k and Supplementary Fig. 3m. (**g**) Gating strategy for Treg apoptosis in Supplementary Fig. 3g. NK natural killer cell, NKT natural killer T cell, DC dendritic cell, Treg regulatory T cell.

Supplementary Tables

Table S1. The clinical characteristics of 10 HCC patients, related to Fig. 1c.

Variable	Number of Patients
Age, year	
<55	1
≥55	9
Gender	
Male	8
Female	2
HBsAg	
Negative	5
Positive	5
Serum AFP, ng/mL	
<400	7
≥400	3
Differentiation Degree	
I-II	7
III-IV	3

Table S2. The clinical and pathological information of 100 patients with HCC, related to Fig. 1f.

Variable	Number of Patients	
	***PON1* expression**	
	Low (n=50)	**High (n=50)**
Age, year		
<55	27	27
≥55	23	23
Gender		
Male	41	43
Female	9	7
HBsAg		
Negative	12	9
Positive	38	41
HCV		
Positive	0	2
Negative	50	48
Serum AFP, ng/mL		
<400	34	27
≥400	16	23
Tumor size (diameter, cm)		
<5	15	21
≥5	35	29
Tumor number		
Single	44	39
Multiple	6	11
Lymph node metastasis		
No	46	50
Yes	4	0
Differentiation Degree		
I-II	29	40
III-IV	21	10

Table S3. The clinical characteristics of 20 HCC patients, related to Figs. 2b, 2c, and 3h.

Variable	Number of Patients	
	***PON1* expression**	
	Low (n=10)	**High (n=10)**
Age, year		
<55	3	4
≥55	7	6
Gender		
Male	10	9
Female	0	1
HBsAg		
Negative	2	2
Positive	8	8
Serum AFP, ng/mL		
<400	7	9
≥400	2	1
Missing	1	0
Differentiation Degree		
I-II	5	9
III-IV	2	1
Missing	3	0

Table S4. The sequence of primers.

Primers sequences for genotyping		
Pon1	F1	AGCATCCCTCTCAGACAGTTAGC
	R1	AAAGTCCTGATATGGAGTGAGCC
	F2	AGCCATCAGTATCATTGTGTGTTTG
Primers for real time PCR		
m *Pon1*	forward	TCCCGGCTCAGAGGTGCTTC
	reverse	GCGACCGTGGTGCCTTGC
m *Hif-1α*	forward	CTGCCACTGCCACCACAACTG
	reverse	TGCCACTGTATGCTGATGCCTTAG
m *Foxp3*	forward	TTTCACCTATGCCACCCTTATC
	reverse	CATGCGAGTAAACCAATGGTAG
m *Sp1*	forward	TCAGCGTCCGCGTTTTTCC
	reverse	ACGCTGTTGACAGGTAGCAA
m *Jun*	forward	AAGAAGCTCACAAGTCCGGG
	reverse	GAGGGCATCGTCGTAGAAGG
m *Nfκb1*	forward	CCCTACGGAACTGGGCAAAT
	reverse	TGCAAATTTTGACCTGTGGGT
m *Srebf2*	forward	GCTGAGGAGTCGTGGGC
	reverse	TCAATCCCGAAAAGAGCGGG
m *Ahr*	forward	AGAGCAACAGCAACAGCTTCAG
	reverse	CGTGTGCTTCGGACCCAGAT
m *Pparg*	forward	TGTGAGACCAACAGCCTGAC
	reverse	GGCATTGTGAGACATCCCCA
m *Actb*	forward	ATCACTATTGGCAACGAGCGGTTC
	reverse	CAGCACTGTGTTGGCATAGAGGTC
H *PON1*	forward	CTTCAGGAACCACCAGTCTTCTTAC
	reverse	GTCCATTAGGCAGTATCTCCAAGTC
H *ACTB*	forward	GGCCAACCGCGAGAAGATGAC
	reverse	GGATAGCACAGCCTGGATAGCAAC

Table S5. Antibodies and stimulants.

Antibodies used for Western blot and Immunofluorescence			
Name	Cat. No.	Co., Ltd	Dilution
PON1	ab92466	Abcam	1:1000
PON1(IF)	ab248121	Abcam	1:100
HIF-1α	ER1802-41	HUABO	1:1000
HIF-1α (IF)	AF02369	AiFang	1:50
VHL	sc-514041	Santa cruz	1:500
Ubiquitin	sc-8017	Santa cruz	1:500
ACTIN	30103ES60	YEASEN	1:5000
Histone H3	sc-517576	Santa cruz	1:500
Tubulin	sc-69971	Santa cruz	1:1000
Stimulants			
Name	Cat. No.	Co., Ltd	
LW6	S8441	Selleck	
Lactic acid	L1750	Sigma	
Quercetin	HY-18085	MCE	
Simvastatin	HY-17502	MCE	
Atorvastatin	HY-B0589	MCE	
Pitavastatin	HY-B0144A	MCE	
TGF-β	CK33	novoprotein	
T5224	HY-12270	MCE	
T0070907	HY-13202	MCE	
AZD3965	HY-12750	MCE	

Table S6. Antibodies used for Flow cytometry.

Antibodies used for Flow cytometry			
Name	Cat. No.	Co., Ltd	Dilution
Pacific Blue anti-mouse CD45	103126	Biolegend	1:100
PE anti-mouse CD4	100408	Biolegend	1:100
Brilliant Violet 510 anti-mouse CD8	100751	Biolegend	1:100
PE-cy7 anti-mouse CD8	25-0088-42	Ebioscience	1:100
APC anti-mouse CD8	MA5-28718	Ebioscience	1:100
PE anti-mouse PD-1	12-9969-42	Ebioscience	1:100
PE-cy7 anti-mouse PD-1	135215	Biolegend	1:100
PE anti-mouse LAG-3	12-2239-42	Ebioscience	1:100
APC/Fire™ 750 anti-mouse LAG-3	125239	Biolegend	1:100
PE anti-mouse Tim3	134003	Biolegend	1:100
APC anti-mouse Tim3	17-3109-42	Ebioscience	1:100
APC anti-mouse IFN-γ	506510	Biolegend	1:50
eFluor 450 anti-mouse IFN-γ	48-7311-82	Ebioscience	1:50
PE anti-mouse TNF-α	506305	Biolegend	1:50
Brilliant Violet 421 anti-mouse TNF-α	404-7321-82	Ebioscience	1:50
Alexa Fluor 647 anti-mouse FOXP3	126407	Biolegend	1:50
APC anti-mouse Annexin V	640919	Biolegend	1:50
FITC anti-mouse Ki-67	652409	Biolegend	1:50
Fixable Viability Dye eFluor 506	65-0866-14	EBioscience	1:200
CD16/CD32 Monoclonal Antibody	14-0161-86	Ebioscience	1:200
APC anti-human CD45	304011	Biolegend	1:100
Brilliant Violet 421 anti-human CD3	317343	Biolegend	1:100
PE anti-human CD4	980804	Biolegend	1:100
FITC anti-human CD8	344703	Biolegend	1:100
PE/Cyanine7 anti-human CD11b	982608	Biolegend	1:100
PE/Dazzle 594 anti-human CD11c	301642	Biolegend	1:100
Brilliant Violet 510 anti-human CD16	302047	Biolegend	1:100
Alexa Fluor 700 anti-human CD56	362521	Biolegend	1:100
Brilliant Violet 785 anti-human CD68	333825	Biolegend	1:100
APC/Cyanine7 anti-mouse/human B220	103223	Biolegend	1:100